Transition path sampling and the calculation of rate constants

Christoph Dellago, Peter G. Bolhuis, Félix S. Csajka, and David Chandler
Department of Chemistry, University of California at Berkeley, Berkeley, California 94720

(Received 5 August 1997; accepted 17 October 1997)

We have developed a method to study transition pathways for rare events in complex systems. The method can be used to determine rate constants for transitions between stable states by turning the calculation of reactive flux correlation functions into the computation of an isomorphic reversible work. In contrast to previous dynamical approaches, the method relies neither on prior knowledge nor on explicit specification of transition states. Rather, it provides an importance sampling from which transition states can be characterized statistically. A simple model is analyzed to illustrate the methodology. © *1998 American Institute of Physics.* [S0021-9606(98)52504-4]

I. INTRODUCTION

The computation of rate constants of dynamical processes dominated by rare events has been the focus of many numerical studies. The traditional method to compute these rates is to identify the transition state of the process as a function of some order parameter, followed by the sampling of molecular simulation trajectories departing from this transition state.[1–4] However, for many systems, in particular complex condensed matter systems, the location of transition states is unknown or not explicitly specifiable. Due to the high dimensionality of the phase space, the energy landscape will be rugged, dense with saddle points and many possible transition states. Further, the order parameter characterizing stable states can be a poor approximation to the reaction coordinate, as illustrated in Fig. 1. These features would present no difficulty if it were possible to sample transition paths statistically, without specific knowledge of the transition state(s). This possibility is the subject of this paper.

Many studies have been devoted to the search of transition paths. For example, there are methods available which locate transition states by looking for explicit individual saddle points in the potential energy landscape.[5–8] This approach is useful for low dimensional systems. In contrast with searching for saddle points directly, other methods beginning with Pratt's proposal,[9] use statistical procedures to find transition pathways between stable states. For complex systems, this approach is a significant step in the right direction. To date, however, applications have employed ad hoc (i.e., non dynamical) rules for the weight governing path statistics.[10–15]

Pratt proposed to use a Markov chain of states between stable states as a stochastic description of the transition path.[9] Usage of explicit deterministic Newtonian trajectories for this purpose is fraught with problems, as the chaotic nature of high dimensional systems makes it very hard to find just the right initial conditions that lead the path over the barrier to the final stable state. Introducing noise or partially averaging over initial conditions can produce path distributions that are not problematical. The paths can be seen as polymers in which subsequent beads represent the state of the system at subsequent time slices, as illustrated in Fig. 1. By moving the whole path through phase space, we may collect an ensemble of representative paths and simultaneously sample physically relevant quantities. The Markov chain for the path can be described by an action, analogous to a discretized quantum path integral action.[16,17]

In Sec. II we introduce the stochastic description of a transition path and the notion of an action representing the path. We derive expressions for the action for two different Markovian transition probabilities, namely, those for Metropolis Monte Carlo and Brownian dynamics. In Sec. III we discuss several methods to sample the action; these are a local Monte Carlo algorithm, configurational bias Monte Carlo, and a dynamical sampling algorithm. In Sec. IV we describe how one can calculate rate constants of a dynamical process dominated by rare events, by using transition path sampling. The results for an illustrative simple model are presented in Sec. V. The model is sufficiently simple that it can be studied by either standard sampling or path sampling. For this model, therefore, we carry out a comparison between the new and traditional methods. Section VI contains the conclusions. As the methodology includes some intricate equations, we use appendices to augment the discussion in the main text.

II. THE ACTION FOR TRANSITION PATHS

A path in space–time is given by an ordered sequence of $L+1$ copies of phase space, $\{x_0 \to x_1 \to \cdots \to x_L\}$, where x_τ denotes a point in $2D$-dimensional phase space (position r_τ, momentum p_τ). The time label is $\tau = 0,1,\ldots,L$; the connection to physical time depends on the nature of the underlying transition rule. The path action therefore depends on $N_p = 2 \times D \times (L+1)$ coordinates.

If consecutive states of the system are linked by a Markovian transition probability $p(x_\tau \to x_{\tau+1})$, the probability for the whole path is given by the product

$$e^{-\beta E(x_0)} \prod_{\tau=0}^{L-1} p(x_\tau \to x_{\tau+1}); \tag{1}$$

here $\beta = 1/k_B T$ and $E(x_\tau)$ is the total energy at x_τ, and the initial time slice is canonically distributed. To sample transition paths, we include the endpoint constraints $h_A(x_0)$ and $h_B(x_L)$ in the path probability:

 0021-9606/98/108(5)/1964/14/$15.00

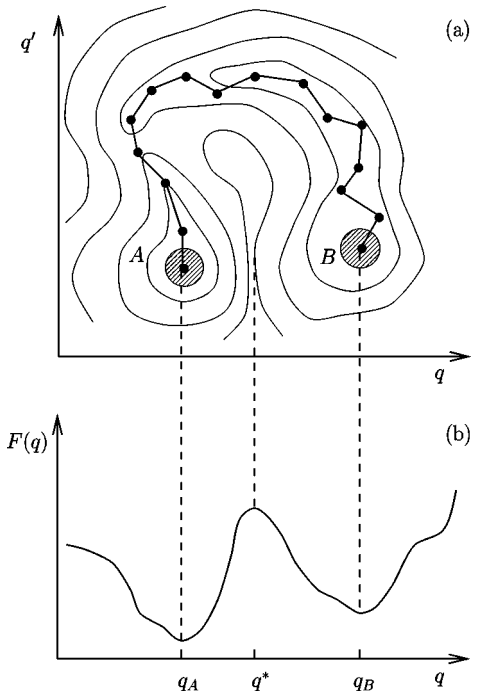

FIG. 1. (a) Schematic energy landscape, $E(q,q')$, with reactant region A and product region B. The chain of beads is a discretized path as used in our path simulation. It reproduces the correct reaction coordinate which depends both on q and on q'. (b) Schematic free energy along coordinate q, $F(q) = -k_B T \log \int dq' \exp\{-\beta E(q,q')\}$. The coordinate q adequately characterizes the stable states near $q=q_A$ and $q=q_B$. The free energy $F(q)$ has a maximum at $q=q^*$. This value of q is far from that associated with the dynamical bottleneck separating the two stable states.

$$\exp(-S[x_0,x_1,\ldots,x_L]) \equiv h_A(x_0) e^{-\beta E(x_0)} \left[\prod_{\tau=0}^{L-1} p(x_\tau \to x_{\tau+1}) \right] h_B(x_L). \tag{2}$$

$h_A(x_0)$ forces the path to start in region A (the reactant region), and $h_B(x_L)$ constrains the path to end in region B (the product region). For this purpose, we choose the characteristic function

$$h_{A,B}(x) = \begin{cases} 1, & \text{if } x \in A,B, \\ 0 & \text{if } x \notin A,B. \end{cases} \tag{3}$$

The evolution from A to B takes place in L steps. Equation (2) defines the action for transition paths.

We are free to choose any Markovian transition probability $p(x_\tau \to x_{\tau+1})$ which conserves the Boltzmann distribution and is normalized.

A. The Metropolis action

The transition probability $p(r \to r')$ for a Markov process generated by the Metropolis Monte Carlo algorithm is

$$p(r \to r') = \omega(r \to r') + \delta(r-r') Q(r), \tag{4a}$$

where

$$\omega(r \to r') = \eta(r,r') \min[1, e^{-\beta(E(r')-E(r))}] \tag{4b}$$

gives the transition probability for an *accepted* new element r' in the Markov chain, and

$$Q(r) = 1 - \int dr'' \omega(r \to r'') \tag{4c}$$

is the probability of *rejecting* a trial move at r. The delta distribution appears because there is a finite rejection probability in the probability density $p(r \to r')$. $\eta(r,r')$ is a symmetric function which decays rapidly for growing $|r-r'|$, for example a Gaussian or a characteristic function with support in a small interval Δr around r (the standard choice in Metropolis Monte Carlo). The min-function returns the smaller of its arguments. The term involving the $Q(r)$ in Eq. (4a), clearly necessary to ensure normalization and a detailed balance, was unfortunately omitted in Pratt's formulation of Monte Carlo chains of states.[9]

The transition probability (4a) corresponds to the well known Metropolis Monte Carlo rule with a generating probability $\eta(r,r')$ and acceptance probability $\min[1, e^{-\beta(E(r')-E(r))}]$.[18] The Metropolis algorithm is in fact an ingenious construction which allows us to avoid the explicit calculation of the rejection probability, $Q(r)$. On the other hand, we then have no control over the endpoints of the trajectory which we generate. In the transition path problem, we want to generate a specific subset of Markov chains which satisfiy the boundary constraints $h_A(r_0)$ and $h_B(r_L)$.

The Metropolis transition probability conserves the canonical ensemble,

$$\int dr e^{-\beta E(r)} p(r \to r') = e^{-\beta E(r')}, \tag{5}$$

and it is normalized by construction.

B. The Langevin action

A many-body system evolving according to the Langevin equation obeys the equations of motion,

$$\begin{aligned} \dot{r} &= v, \\ m\dot{v} &= F(r) - \gamma p + \mathcal{R}, \end{aligned} \tag{6}$$

where r and $p=mv$ denote the positions and momenta of the particles, respectively, $F=-\partial V/\partial r$ is the intermolecular force, and γ is a friction coefficient. The state of the system at time τ is given by $x_\tau \equiv \{r_\tau, v_\tau\}$. The random force $\mathcal{R}$, which is assumed to be a Gaussian random variable uncorrelated in time,[19] $\langle \mathcal{R}(t)\mathcal{R}(0)\rangle = 2m\gamma k_B T \delta(t)$, acts as a heat bath compensating for the energy dissipated by the frictional term $-\gamma p$. Consequently, trajectories evolving according to the Langevin equation conserve the canonical ensemble. Furthermore, the random coupling to the heat bath introduces a stochastic element into the dynamics of the system ''smearing out'' its deterministic trajectory. Therefore, the time evolution of the system during a short time Δt consists of a systematic part δx_S and a random part δx_R induced by the stochastic force:

$$x_{\tau+1} = x_\tau + \delta x_S + \delta x_R. \tag{7}$$

Hence, the probability for a transition from x_τ to $x_{\tau+1}$ is given by

$$p(x_\tau \to x_{\tau+1}) = w(\delta x_R), \tag{8}$$

where $w(\delta x_R)$ is the probability distribution of the random displacement δx_R. For given endpoints x_τ and $x_{\tau+1}$ the random part δx_R can be obtained from Eq. (7), where the systematic part δx_S must be evaluated with an appropriate integrator. We refer the reader to Appendix A for an efficient scheme to determine δx_S for Langevin dynamics. By concatenating L short-time transition probabilities (8) one finally obtains the probability of a path of length $\mathscr{T} = L\Delta t$.

As shown by Chandrasekhar,[19] the distribution w of the random displacements δx_R can be calculated analytically if the dynamics of the system is governed by the equations of motion (6):

$$w(\delta x_R) = \left(2\pi\sigma_r\sigma_v\sqrt{1-c_{rv}^2}\right)^{-D} \times \prod_{\alpha=1}^{D} \exp\left\{-\frac{1}{2(1-c_{rv}^2)}\left[\left(\frac{\delta r_R^\alpha}{\sigma_r}\right)^2 + \left(\frac{\delta v_R^\alpha}{\sigma_v}\right)^2 - 2c_{rv}\left(\frac{\delta r_R^\alpha}{\sigma_r}\right)\left(\frac{\delta v_R^\alpha}{\sigma_v}\right)\right]\right\}, \tag{9}$$

where $\delta x_R = \{\delta r_R, \delta v_R\}$ and α denotes the different components of the displacement vectors δr_R and δv_R. Since the components of the random force are assumed to be uncorrelated also the components of the random displacements are independent from each other. However, the bivariate distribution (9) couples the configuration and momentum components, δr^α and δv^α, of the random displacement. The variances σ_r and σ_v and the correlation coefficient c_{rv} are given by

$$\sigma_r^2 = \Delta t\,\frac{k_B T}{m\gamma}[2-(3-4e^{-\gamma\Delta t}+e^{-2\gamma\Delta t})/\gamma\Delta t],$$

$$\sigma_v^2 = \frac{k_B T}{m}(1-e^{-2\gamma\Delta t}), \tag{10}$$

$$c_{rv}\sigma_r\sigma_v = \frac{k_B T}{m\gamma}(1-e^{-\gamma\Delta t})^2.$$

In the limit of high friction the inertial term in the equation of motion (6) can be neglected, leading to the simplified equation

$$m\gamma\dot{r} = F(r) + \mathscr{R}. \tag{11}$$

Accordingly, the system at time slice τ corresponding to $t = \tau\Delta t$ is completely defined by its position coordinates r_τ. In this case, the random displacement δr_R is distributed according to[20]

$$w(\delta r_R) = \prod_{\alpha=1}^{D} \frac{1}{\sigma_r(2\pi)^{1/2}}\exp\left\{-\frac{(\delta r_R^\alpha)^2}{2\sigma_r^2}\right\}, \tag{12}$$

where the variance σ_r is given by

$$\sigma_r^2 = 2\,\frac{k_B T}{m\gamma}\Delta t. \tag{13}$$

In contrast to the Metropolis transition probability, the Langevin transition probability is a smooth function of the endpoints of the path. This feature makes the Langevin transition probability suitable for the application of the dynamical algorithms presented in subsequent sections.

III. SAMPLING THE DISTRIBUTION OF PATHS

The definition (2) of the action makes the path probability analogous to the canonical distribution for a polymer system:

$$\exp\{-S\} \leftrightarrow \exp\{-\beta V\}. \tag{14}$$

V is the potential energy of the polymer system depending on all the configuration coordinates. In the path case the action S plays the role of the potential energy V multiplied by the inverse temperature β.

In the following sections we exploit this isomorphism and adapt Monte Carlo methods and dynamical methods originally developed to sample the canonical probability density of many-particle systems to the path sampling problem.

A. Monte Carlo algorithms

Monte Carlo algorithms for transition path sampling can be derived in analogy to polymer Monte Carlo methods. The simplest representative is the local algorithm, which makes trials for each time slice individually. In contrast, the configurational bias Monte Carlo (CBMC) algorithm attempts to regrow the entire path in one step. To increase the probability that the regrown path reaches region B, we guide the path towards B with a guiding field.

1. Local algorithm

A local Monte Carlo algorithm samples each time slice individually. The acceptance probability for a change in an intermediate time slice τ is

$$P_{\rm acc}[x_\tau \to x'_\tau] = \min\left[1, \frac{P_{\rm gen}[x_\tau]}{P_{\rm gen}[x'_\tau]}\,\frac{\exp(-S[x_0,\ldots,x'_\tau,\ldots,x_L])}{\exp(-S[x_0,\ldots,x_\tau,\ldots,x_L])}\right] = \min\left[1, \frac{P_{\rm gen}[x_\tau]}{P_{\rm gen}[x'_\tau]}\,\frac{p(x_{\tau-1}\to x'_\tau)p(x'_\tau\to x_{\tau+1})}{p(x_{\tau-1}\to x_\tau)p(x_\tau\to x_{\tau+1})}\right], \tag{15}$$

where $P_{\rm gen}[x'_\tau]$ is the *a priori* generating probability for the trial move x'_τ. We refer to the phase space variables, x_τ, in Eq. (15) to emphasize that the Monte Carlo sampling of paths applies in principle to paths, either in configuration space or phase space. In this paper, however, our use of Monte Carlo sampling is confined to configuration space, with variables r_τ.

In constructing a local algorithm for the Metropolis path action, one faces the problem that $p(r\to r')$ contains a singular part $\delta(r-r')Q(r)$. $P_{\rm gen}[r'_\tau]$ should be chosen in a manner that creates rejected steps in the Markov chain with a finite probability. This can be achieved with the following rule:

$$P_{\mathrm{gen}}[r'_\tau]=\frac{g(r_\tau,r'_\tau)+\delta(r'_\tau-r_{\tau-1})Q(r_{\tau-1})+\delta(r'_\tau-r_{\tau+1})Q(r_{\tau+1})}{|g|(r_\tau)+Q(r_{\tau-1})+Q(r_{\tau+1})}. \tag{16}$$

$g(r,r')$ generates trials r' which correspond to accepted trial steps in the underlying Metropolis Markov chain. It is a rapidly decaying function with finite norm $|g|(r)=\int dr' g(r,r')$; we use a Gaussian with width σ_g, i.e., $g(r,r')=\exp\{-(r-r')^2/(2\sigma_g^2)\}$. The generating probability (16) simplifies the acceptance rule [Eq. (15)] considerably; in particular, the delta distributions will always arise in pairs in the numerator and the denominator. We rewrite Eq. (15) in the form

$$P_{\mathrm{acc}}[r_\tau\to r'_\tau]=\min[1,A/B]; \tag{17}$$

where

$$A=\begin{cases}\omega(r_{\tau-1}\to r_{\tau+1}), & \text{if } r'_\tau=r_{\tau-1} \text{ or } r'_\tau=r_{\tau+1};\\ \omega(r_{\tau-1}\to r'_\tau)\,\omega(r'_\tau\to r_{\tau+1})/g(r_\tau,r'_\tau), & \text{otherwise.}\end{cases}$$
$$B=\begin{cases}\omega(r_{\tau-1}\to r_{\tau+1}), & \text{if } r_\tau=r_{\tau-1} \text{ or } r_\tau=r_{\tau+1};\\ \omega(r_{\tau-1}\to r_\tau)\,\omega(r_\tau\to r_{\tau+1})/g(r_\tau,r'_\tau), & \text{otherwise.}\end{cases} \tag{18}$$

The algorithm above holds for all intermediate time slices; Appendix B gives the local algorithm for the endpoints r_0 and r_L.

While correct in principle, the local algorithm scales with L^3 (Ref. 17) and hence equilibrates very slowly. Collective moves of the path can improve this sampling efficiency by one or more powers of L.

2. Configurational bias sampling

The CBMC method samples equilibrium conformations of a polymer by regrowing the entire chain in a biased fashion:[21] since a chain generated at random is very likely to overlap with itself and/or with its neighbors, each segment is regrown with a bias proportional to its Boltzmann weight. There is a correction for the biased growth called the Rosenbluth weight which enters the acceptance probability in the CBMC algorithm. The Rosenbluth weight is defined as the ratio $W_a=P_a/e^{-S_a}$, where P_a is the total CBMC generating probability of path a, and S_a is a's path action. The detailed balance condition immediately leads to $P_{\mathrm{acc}}(a\to b)=\min[1,W_b/W_a]$.

For free paths [with trivial boundary constraints $h_A(r_0)=1$ and $h_B(r_L)=1$], it is possible to generate new paths which will be accepted with probability one. The CBMC generating probability is proportional to the Markovian transition probability; for each time slice, one generates k trials $\{r_\tau^{(i)}\}$, $i=1,\ldots,k$ at random and calculates the transition probability $p(r_{\tau-1}\to r_\tau^{(i)})$.

Since the endpoint constraint $h_B(r_L)$ is seldom satisfied for an unbiased path, we use a generating probability which includes a guiding field. This idea has been introduced in a slightly different context by Garel and Orland.[22,23] It makes use of the identity

$$\prod_{\tau=0}^{L-1} p(r_\tau\to r_{\tau+1})=\prod_{\tau=0}^{L-1} p(r_\tau\to r_{\tau+1})\exp[\phi_\tau(r_\tau)-\phi_{\tau+1}(r_{\tau+1})], \tag{19}$$

where the guiding field ϕ_τ can be any function satisfying $\phi_0=0$ and $\phi_L=0$. The generating probability $\tilde{P}_{\mathrm{gen}}[r'_\tau]$ in the guiding field scheme is proportional to $p(r_{\tau-1}\to r'_\tau)\times\exp[\phi_{\tau-1}(r_{\tau-1})-\phi_{\tau'}(r_{\tau'})]$. The acceptance probability has to be changed in accordance to $\tilde{P}_{\mathrm{gen}}[r'_\tau]$; the choice for the guiding field strongly affects the efficiency of the algorithm. Further details concerning the CBMC algorithm with a guiding field are in Appendix B. Finally, one can also define a guiding force as the negative gradient of the guiding field. The guiding force can be used to construct a CBMC-like scheme for Langevin paths.

B. Dynamical algorithms

CBMC methods are only one of the possible techniques that improve upon local MC algorithms. One can, for example, speed up the simulation considerably by adopting smart MC methods which use the gradient of the action $S(X)$ as additional information.[20] Alternatively, one may use a dynamical algorithm capable of generating paths according to their action in an efficient way. It is, however, important to keep in mind that the artificial dynamics of the path is completely different from the real dynamics of the original system *along* the path. The former is nothing more than a convenient method to generate paths according to their action and has no physical meaning. We note that similar methods have been used for the evaluation of quantum path integrals and fermionic determinants.[24,25]

By taking the analogy (14) one step further, we define a momentum P conjugate to the path coordinates $X\equiv\{x_0,\ldots,x_L\}$ and complement the action with the related artificial kinetic energy obtaining the path Hamiltonian,

$$H_{\mathrm{P}}(X,P)=\sum_{\alpha=0}^{N_{\mathrm{P}}}\frac{P_\alpha^2}{2M}+S(X). \tag{20}$$

$N_{\mathrm{P}}=2D(L+1)$ is the dimension of the path space and M is an artificial mass associated with the path. P_α denotes the artificial momentum conjugated to the degree of freedom α

of the path. The following equations in artificial time θ derived from the path Hamiltonian (20) move the path through path space at constant H_P:

$$\dot{X} \equiv \partial H_P / \partial P = P/M,$$
$$\dot{P} \equiv -\partial H_P / \partial X = -\nabla_X S(X). \tag{21}$$

Here, the dot denotes the derivative with respect to the artificial time θ. Since these equations of motion conserve the path Hamiltonian H_P, a path-trajectory generated by (21) does not visit points in phase space according to $\exp\{-S[x_0,...,x_L]\}$. If, however, one occasionally selects one or more degrees of freedom and redraws the associated path momenta P_α from the Maxwell–Boltzmann distribution,

$$\rho(P_\alpha) = \frac{1}{\sqrt{2\pi M}} \exp\left\{ -\frac{P_\alpha^2}{2M} \right\}, \tag{22}$$

the path samples the correct distribution. Between these random events the time evolution of the path is governed by the equations of motion (21). This stochastic method, which is known as the Andersen thermostat, corresponds to coupling the path to an imaginary heat bath with a temperature of 1. It is based on a kinetic model due to Bohm and Gross,[26,27] subsequently popularized by Andersen.[28] At each collision with the heat bath the path is hopping between shells corresponding to different values of H_P, visiting the path space with the correct probability. A similar method consists in using the Langevin equation to move the path through path space.[29] Alternatively, to generate a canonical distribution of paths one may apply deterministic thermostats like the Nosé–Hoover thermostat[30,31] or the Gaussian isokinetic thermostat.[32,33] However, these thermostats fail to sample the canonical distribution ergodically if the forces are nearly harmonic, as is the case for path forces $-\boldsymbol{\nabla}_X S(X)$ derived from the Langevin transition probability.

The integration of the equations of motion (21) requires the calculation of the path forces $-\nabla_X S(X)$. Writing the action as

$$S = \beta E(x_0) - \sum_{\tau=0}^{L-1} \log p(x_\tau \to x_{\tau+1}) - \log h_A(x_0) - \log h_B(x_L) \tag{23}$$

makes clear that different path forces arise from the canonical distribution of states in the first time slice, the chain of transition probabilities linking adjacent time slices, and the initial and final constraint on the path. If the regions A and B are described by the characteristic functions (3) the endpoints of the paths are confined to their respective regions by containers with hard walls. The combination of all forces leads to a path trajectory in artificial time consisting of smooth streaming segments interrupted by impulsive collisions of the path endpoints with the constraining boundaries. In Appendix C we give a detailed description of the path forces. Furthermore, we derive appropriate collision rules for the path endpoints and explain how to combine them with the smooth flow of the system between collisions.

IV. CALCULATING RATE CONSTANTS

The calculation of rate constants is one of the most important goals of numerical studies of dynamical processes. In this section, we use correlation function formulas to relate the rate constant to transition path sampling. Further, we use these formulas to determine the path length L sufficient to adequately sample the ensemble of transition paths. The phenomenological rate constants can be related to microscopic averages using the fluctuation–dissipation theorem (see for example Ref. 3),

$$k(t) \equiv \frac{\langle h_A(x(0)) \dot{h}_B(x(t)) \rangle}{\langle h_A(x(0)) \rangle} \approx k_{A\to B} \exp(-t/t_{\mathrm{rxn}}), \tag{24}$$

where h_A and h_B are the characteristic functions for the stable states as defined in Eq. (3), the dot denotes the time derivative of the function, and $t_{\mathrm{rxn}}^{-1} = k_{A\to B} + k_{B\to A}$ is the relaxation time with $k_{A\to B}$ and $k_{B\to A}$ as the forward and backward reaction rate constants, respectively. The brackets $\langle \cdots \rangle$ indicate ensemble everages. In the above equation, it is assumed that $\langle h_A \rangle + \langle h_B \rangle \approx 1$, which reflects the fact that—because of a high free energy barrier—the system is nearly always in one of the stable states and hardly ever at the top of the barrier.

The correlation function in Eq. (24) is the time derivative of the probability for the system to be in region B at time t provided it was in region A at time 0. For barriers large compared to $k_B T$, the function reaches a plateau after a certain short molecular relaxation time $t_{\mathrm{mol}} \ll t_{\mathrm{rxn}}$. Because of this separation of time scales, $\exp(-t/t_{\mathrm{rxn}}) \approx 1$ in this region, and the function $k(t)$ is equal to the phenomenological rate constant $k_{A\to B}$ we want to calculate.

The correlation function $k(t)$, however, is not conveniently formulated for the transition path method. We therefore change to a discrete representation of time in which the time slices are labeled by $\tau = t/\Delta t$. Subsequently, we factorize $k(\tau \Delta t)$ as

$$k(\tau \Delta t) = \nu(\tau) P(L), \tag{25}$$

where L is the total number of time slices of the path,

$$\nu(\tau) = \frac{\langle h_A(x_0) \dot{h}_B(x_\tau) \rangle}{\langle h_A(x_0) h_B(x_L) \rangle} \approx \frac{\langle h_A(x_0) \dot{h}_B(x_\tau) h_B(x_L) \rangle}{\langle h_A(x_0) h_B(x_L) \rangle} \equiv \langle \dot{h}_B(x_\tau) \rangle_{AB}, \tag{26}$$

and

$$P(L) = \frac{\langle h_A(x_0) h_B(x_L) \rangle}{\langle h_A(x_0) \rangle} \equiv e^{-W(L)}. \tag{27}$$

The average $\langle \dot{h}_B(x_\tau) \rangle_{AB}$ is the time derivative of the probability that on a path between A and B, region B will be reached after τ time steps. The subscript AB indicates that the initial and final constraints are included in the transition path ensemble average. The approximate equality of Eq. (26) can be explained as follows. By defining $h_{\tilde{B}}(x) = 1 - h_B(x)$ we can write

$$\langle h_A(x_0)\dot{h}_B(x_\tau)\rangle = \langle h_A(x_0)\dot{h}_B(x_\tau)(h_B(x_L)+h_{\tilde{B}}(x_L))\rangle \approx \langle h_A(x_0)\dot{h}_B(x_\tau)h_B(x_L)\rangle, \tag{28}$$

where we make use of the fact that $t_{\mathrm{mol}} < L\Delta t \ll t_{\mathrm{rxn}}$. Once the path has reached region B it will stay there for a long period on the scale of t_{mol} and we can therefore neglect the contribution of $\langle h_A(x_0)\dot{h}_B(x_\tau)h_{\tilde{B}}(x_L)\rangle$.

Since the factor $P(L)$ in Eq. (25) does not depend on τ, we expect $\nu(\tau)$ to reach a plateau value after a certain time t_{mol}. This plateau value is to be used in the calculation of the rate constant $k_{A\to B}$. In fact, we can use this as a criterion to check if our transition path is long enough, i.e., consists of a sufficient number of time slices to capture the most likely transition paths.

The function $P(L)$ is the probability a path initiated in region A will reach region B in L time steps. In principle, this average could be calculated by an ordinary simulation which starts in A. However, for large barriers the probability to reach B in L time steps is vanishingly small. An attempt to use directed path simulation in a straightforward way (without the constraint for the endpoint) would also suffer from extremely poor statistics.

It is illuminating to interpret the function $W(L)$ we introduced in Eq. (27) as the isomorphic reversible work needed to constrain the endpoint (time slice L) of the path to region B. This analogy allows us to invoke techniques that have been developed for the calculation of the free energy in complex systems.

One way to make the calculation of $P(L)$ numerically tractable is using a method related to umbrella sampling.[34,35] We divide the phase space in several regions or ''windows'' B_λ, where λ is a parameter characterizing the region. We perform path simulations in which the constraint for initial region A remains fixed, but in which the final region is defined by B_λ. For every simulation we divide this phase space region B_λ into a (large) number of thin shells and histogram the probability to find the endpoint in these shells. These histograms are not normalized but have an unknown prefactor because endpoints outside region B_λ are excluded in the simulation. Matching the histograms of each window results in a ''master histogram'' representing the entire probability distribution of finding the endpoint in the shell characterized by parameter λ. The desired correlation function $P(L)$ or equivalently the reversible work function $W(L)$ is then easily found by integration.

Alternatively, one can use thermodynamic integration to calculate $W(L)$,

$$-W(L) = \ln \frac{\langle h_A(x_0)h_B(x_L)\rangle}{\langle h_A(x_0)\rangle} = \int_0^1 d\lambda \frac{d}{d\lambda}\ln\langle h_A(x_0)h_B^{(\lambda)}(x_L)\rangle. \tag{29}$$

As in umbrella sampling we perform path simulations in which the constraint for initial region A remains fixed, but in which we vary the size of final region B as a function of a parameter λ. Starting with a final region B_λ which comprises the whole of phase space, we gradually decrease the size of region B_λ until we reach the original final region. If the characteristic function $h_B^{(\lambda)}$ is a continuous function, we can simply sample the derivative in the integrand of Eq. (29). In case of a discontinuous characteristic function one cannot take the analytical derivative, because the only influence of the constraint lies in the path momentum reversal upon collision with the constraint wall. However, we can circumvent this problem by writing the derivative as

$$\frac{d}{d\lambda}\ln\langle h_A(x_0)h_B^{(\lambda)}(x_L)\rangle = \lim_{\Delta\lambda\to 0}\frac{1}{\Delta\lambda}\frac{\langle h_A(x_0)h_B^{(\lambda+\Delta\lambda)}(x_L)\rangle - \langle h_A(x_0)h_B^{(\lambda)}(x_L)\rangle}{\langle h_A(x_0)h_B^{(\lambda)}(x_L)\rangle}. \tag{30}$$

The fraction in the last equation denotes the probability to find the endpoint in an infinitesimal shell in phase space between region B_λ and $B_{\lambda+d\lambda}$. In the dynamical path integration scheme this is equal to the fraction of time the endpoint spends in that shell. If the thickness of the shell is infinitesimal small the time $d\theta$ spent in the shell is inversely proportional to the artificial velocity of the endpoint normal to the shell boundary,

$$d\theta = 2\frac{dr(\lambda)}{v_L\cdot\hat{n}}. \tag{31}$$

Here, $dr(\lambda)$ is the thickness of the shell as a function of λ, v_L is the artificial velocity of the endpoint in path space, and $\hat{n}$ is the inwards directed normal to the boundary of region B_λ. Both v_L and $\hat{n}$ have the dimensionality of the phase space of the system. Summing over the collisions leads to the desired fraction:

$$\frac{d}{d\lambda}\ln\langle h_A(x_0)h_B^{(\lambda)}(x_L)\rangle = \frac{1}{d\lambda}\frac{1}{\Theta}\sum_{\mathrm{coll}} d\theta = \frac{2}{\Theta}\frac{dr(\lambda)}{d\lambda}\sum_{\mathrm{coll}}\frac{1}{v_L\cdot\hat{n}}, \tag{32}$$

where Θ is the total artificial time of the simulation. Substituting Eq. (32) in Eq. (29) we obtain

$$-W(L) = \ln\frac{\langle h_A(x_0)h_B(x_L)\rangle}{\langle h_A(x_0)\rangle} = \int_0^1 d\lambda\frac{2}{\Theta}\frac{dr(\lambda)}{d\lambda}\sum_{\mathrm{coll}}\frac{1}{v_L\cdot\hat{n}}. \tag{33}$$

This expression can be evaluated by performing several simulations for different values of λ, measuring the integrand and finally calculating the integral over λ numerically.

V. NUMERICAL ILLUSTRATIONS

A. Model potential

In this section, we illustrate the consistency of the path sampling method with standard simulation techniques. For

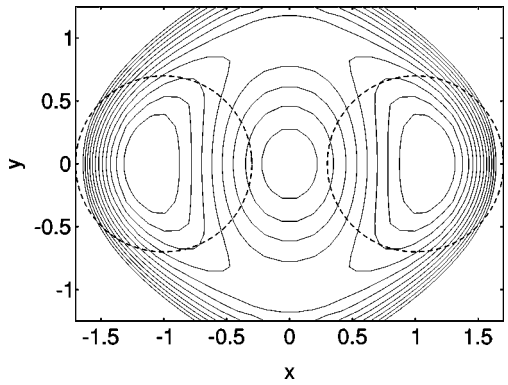

FIG. 2. Contour lines of the two-dimensional model potential used in the numerical simulations. The dashed circles mark the initial and final region with radius $R=0.7$ centered around $(-1,0)$ and $(1,0)$.

simplicity, we consider a system consisting of one particle in the following simple two-dimensional potential:

$$V(x,y)=(4(1-x^2-y^2)^2+2(x^2-2)^2+((x+y)^2-1)^2 +((x-y)^2-1)^2-2)/6. \tag{34}$$

Throughout the paper we use reduced units. As can be seen in Fig. 2, the potential has two minima separated by a barrier. At the barrier there are two transition states. In all the simulations discussed in this section, the reciprocal temperature was $\beta=8$. The corresponding temperature is still high enough to allow the reproduction of transition path simulations by unconstrained methods. For the rate constant to exist, particles must remain most of the time in one of the stable states. Therefore, we chose the initial and final region such that at the temperature under consideration the particle stays 99% of the time in either region A or B. The initial and final region are defined as circles with a radius of $R=0.7$ centered around $(x=\pm 1, y=0)$ as indicated in the figure.

B. Path sampling

We performed three types of Monte Carlo sampling to generate a transition path ensemble governed by the Metropolis action for a particle in the double well potential: a straightforward Metropolis Monte Carlo simulation, a local algorithm path simulation and a CBMC path simulation. All three methods have the following features in common: The number of time slices was $L=30$ and $\eta(r,r')$ was chosen to be Gaussian such that $\eta(r,r')\propto\exp\{-(r-r')^2/(2\sigma^2)\}$, $\sigma=0.25$.

In the straightforward MC simulations we set $P_{\text{gen}}(r,r')=\eta(r,r')$, and the first time slice was sampled according to a canonical distribution subject to the constraint $h_A(r_0)$. After every 50 Monte Carlo moves a MC trajectory of L steps was shot off. Only those trajectories that ended in the final region were taken into account in the averaging. With this procedure, we find an acceptance rate of 1.26×10^{-4} for trial paths.

The local algorithm simulations were performed with $g(r,r')=\exp\{-(r-r')^2/(2\sigma^2)\}$, $\sigma=0.25$, resulting in an acceptance probability of 59%. The rejection factor $Q(r)$ was estimated by MC-integration, where 100 trial displacements were drawn from the Gaussian distribution $\eta(r,r')$.

The CBMC runs use a guiding field $\exp\{-\phi_\pi(r)\}=\exp\{\beta^*V(r)\}$ with $\beta^*=2.5$, except for the endpoints where $\exp\{-\phi_\pi\}=1$. This particular guiding field was chosen after studying the convergence of the energy profile for different choices of β^*. A series of short runs shows poor convergence for smaller or larger values of β^* because the rate of acceptance is low. The upper summation limit is $k=100$. With this choice, about 0.3% of the CBMC trial paths reach the final region, and the overall acceptance rate is 6×10^{-4}.

Both the local and the CBMC algorithm simulations were performed for 10^7 passes. One pass is an average of one trial move for each time slice for the local algorithm and one attempt to grow a path for the CBMC algorithm. Both algorithms require about the same amount of CPU time per pass, since the estimation of the rejection factor $Q(r)$ (local algorithm) and the trial moves for each time slice (CBMC) are the time-consuming operations in each case.

The consistency of the path simulations with a straightforward MC simulation using the same parameters can be tested by comparing the average potential energy and the energy fluctuation. In Fig. 3 the potential energy and the energy fluctuations are plotted as a function of the time slice label for the two path algorithms and the straightforward method. The agreement is excellent, thus validating the usage of MC path sampling. We note that the maximum of the potential energy profile is below the transition state value. The maximum of the potential energy of an individual path does not occur at a specific time slice but shifts for different realizations of the transition path. Therefore the averaging over the path ensemble smears out the potential energy profile.

In case of the dynamical algorithms, we compared the Langevin path dynamics using the Andersen thermostat with straightforward Brownian dynamics. Both the high friction limit as well as the case including inertia (full Langevin equation) were investigated. Starting with the high friction limit, the parameters were as follows. The time step on the Langevin level was $\Delta t=0.15$, the friction coefficient was $\gamma=3$, and the length of the path $L=199$. On the path level the artificial time increment was $\delta t=0.01$, the momentum re-initialization in the Andersen thermostat was done every 200 time steps on average. 4×10^7 integration steps were needed to obtain an accurate estimate of the potential energy averages.

For the straightforward simulation we used high friction Brownian dynamics with the above parameters, while averaging the potential energies over all trajectory segments connecting region A to region B in $L=199$ time steps. The results for the potential energy and the fluctuations of the potential energy are plotted in Fig. 4. Again, the agreement is excellent.

Next, we consider the paths evolving according to the full Langevin equation. The time step on the Langevin level was $\Delta t=0.25$, the number of time slices $L=80$ and the friction was $\gamma=2.5$. On the path level the artificial time incre-

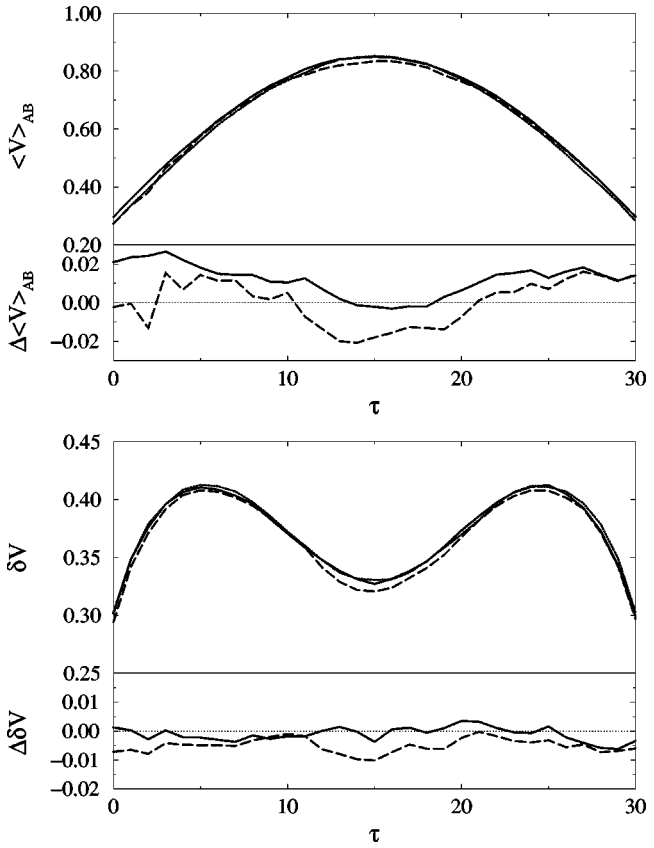

FIG. 3. Profile of the potential energy $\langle V\rangle_{AB}$ (top figure) and of the fluctuations of the potential energy $\delta V=(\langle V^2\rangle_{AB}-\langle V\rangle_{AB}^2)^{1/2}$ (bottom figure) along Monte Carlo transition paths of length $L=30$ and $\beta=8$. The index τ numbers the time slices. The solid line refers to results of the local algorithm (10^7 MC passes), the dashed line to results with the CBMC algorithm (10^7 MC passes), and the dotted line was obtained from a straightforward Metropolis Monte Carlo simulation. The lower parts of the figures show the differences between the path sampling results and the results of the straightforward Monte Carlo simulations both for the local algorithm (solid line) and the CBMC algorithm (dashed line).

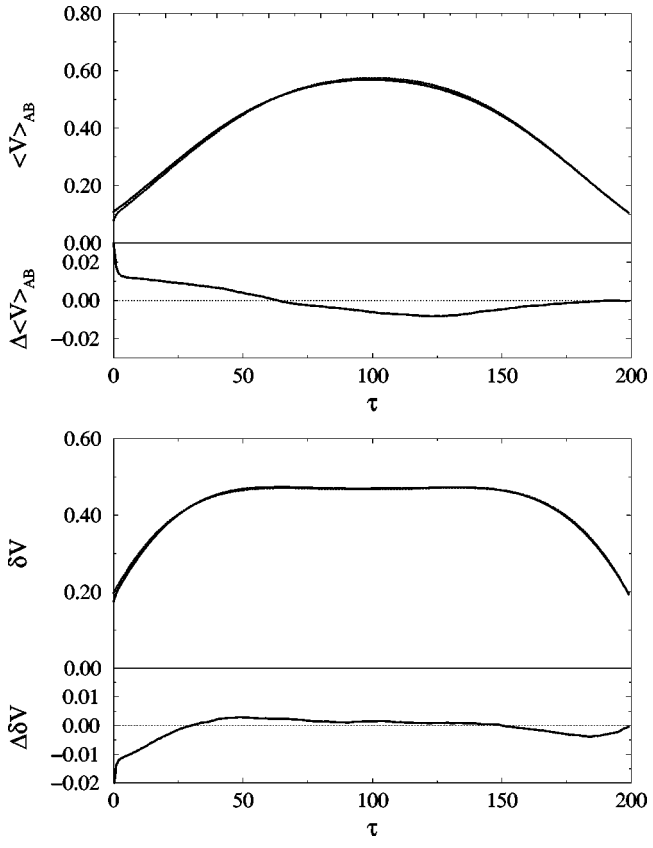

FIG. 4. Average of the potential energy $\langle V\rangle_{AB}$ (top figure) and of the fluctuations of the potential energy $\delta V=(\langle V^2\rangle_{AB}-\langle V\rangle_{AB}^2)^{1/2}$ (bottom figure) along transition paths of length $L=199$ for Langevin dynamics in the high friction limit. The index τ numbers the time slices. The solid line refers to results of a path sampling simulation whereas the dotted line was obtained from a Brownian dynamics trajectory. For both simulations $\beta=8$ and $\gamma=3.0$. The lower parts of the figures show the differences between the path sampling results and the results of the Brownian dynamics simulations.

ment was $\delta t=0.005$, the Andersen update frequency was once every 2000 time steps on average. About 5×10^7 integration steps were needed to obtain an accurate estimate of the potential energy averages. We compare the results of the path sampling simulation with averages obtained from a Brownian dynamics trajectory of 10^9 steps using the same parameters as for the path sampling. Again, we averaged over all trajectory segments connecting A and B. In Fig. 5 we plot the average potential energy and the fluctuations of the potential energy along the path. As in the previous two comparisons, the agreement is excellent.

The scaling of the simulation time needed to obtain a certain accuracy with the path length L can be studied by computing the time correlation function $\langle O(0)O(t)\rangle$ for a relevant quantity O. For the Monte Carlo algorithms, t is the number of cycles, whereas for the dynamical algorithms, t refers to the artificial time of the path dynamics. We studied the time correlation of the potential energy $V(\tau)$ and the function $h_B(x_\tau)$ at different time slices τ along the path. An analysis of typical decay times of the autocorrelation functions showed that the simulation time is proportional to L^3 for the local MC algorithm, whereas it grows with L^2 in the case of the dynamical algorithms. Of course, the correlation functions $\langle O(0)O(t)\rangle$ can also be used to estimate the errors in the averages $\langle O\rangle$.

Another way to estimate the accuracy of the algorithm is to study cumulative averages of relevant quantities as a function of the simulation time. Figure 6 shows the cumulative averages of the potential energy at different time slices τ along the path as a function of the number of integration time steps. The data shown in the picture were obtained from a path simulation for the full Langevin equation with $L=80$, $\beta=8$, and $\gamma=2.5$. The integration time step was $\Delta t=0.05$. As can be inferred from the figure, the accuracy of the potential energy averages is of the order of 1%.

C. Rate constant calculation

We estimate the rate constant for the double well potential (34) using the path sampling algorithms and compare it to straightforward calculations. Two different methods are considered: (1) umbrella sampling and (2) thermodynamic integration.

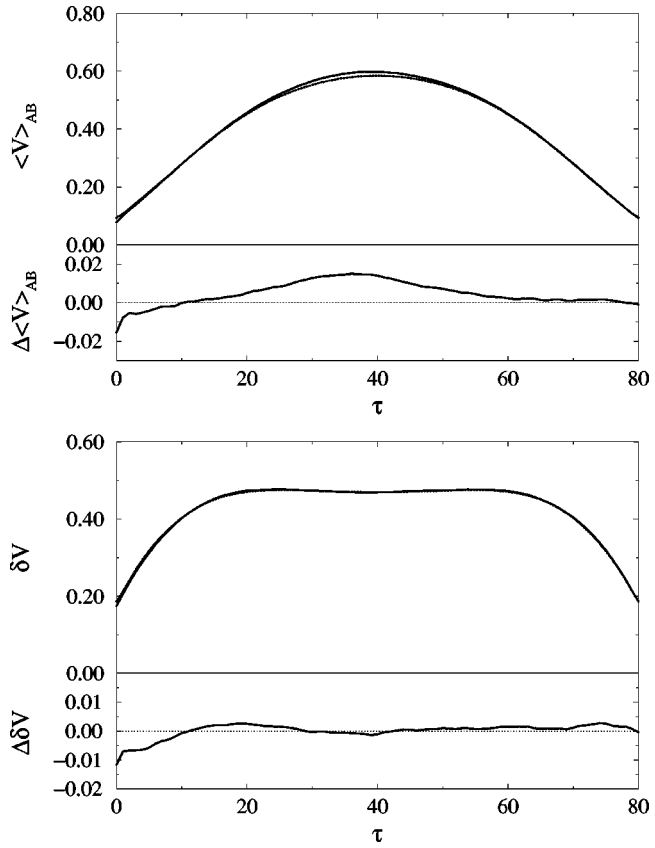

FIG. 5. Average of the potential energy $\langle V\rangle_{AB}$ (top figure) and of the fluctuations of the potential energy $\delta V=(\langle V^2\rangle_{AB}-\langle V\rangle_{AB}^2)^{1/2}$ (bottom figure) along transition paths of length $L=80$ for Langevin dynamics including inertial terms. The index τ numbers the time slices. The solid line refers to results of a path sampling simulation whereas the dotted line was obtained from a Brownian dynamics trajectory, where 1000 transitions occurred during the simulation. For both simulations $\beta=8$ and $\gamma=2.5$. The lower parts of the figures show the differences between the path sampling results and the results of the Brownian dynamics simulations.

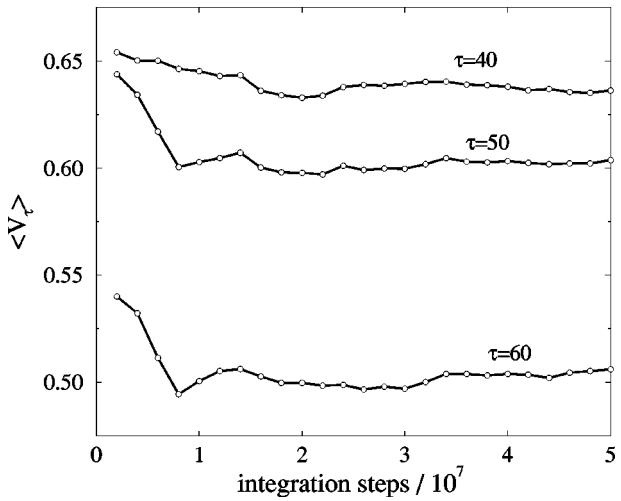

FIG. 6. Cumulative average of the potential energy $\langle V\rangle_{AB}$ at different time slices τ along the path as a function of the number of integration time steps. Transition paths of length $L=80$ corresponding to the full Langevin equation with $\beta=8$ and $\gamma=2.5$ were studied.

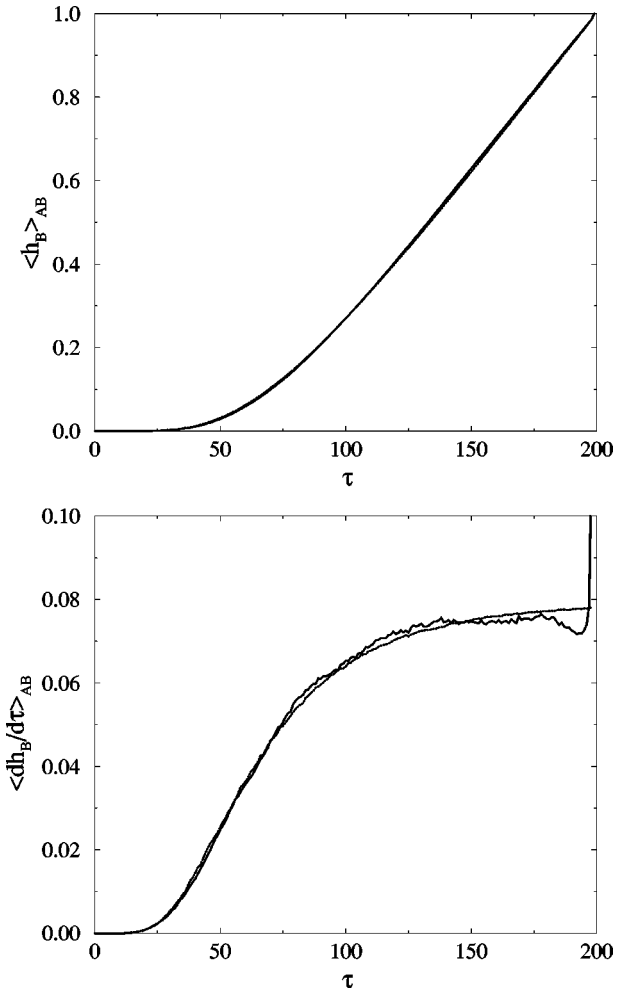

FIG. 7. Normalized correlation function $\langle h_B(x_\tau)\rangle_{AB}$ (top figure) and its time derivative $\langle \dot{h}_B(x_\tau)\rangle_{AB}$ (bottom figure) along transition paths of length $L=199$ for Langevin dynamics in the high friction limit. The index τ numbers the time slices. The solid line refers to results of a path sampling simulation whereas the dotted line was obtained from a Brownian dynamics trajectory. For both simulations $\beta=8$ and $\gamma=3.0$.

Case 1: We apply the umbrella sampling method described in Sec. IV to the high friction case. First, we focus on the $\nu(\tau)=\langle \dot{h}(\tau)\rangle_{AB}$ and its integral $\tilde{k}(\tau)=\langle h_B(\tau)\rangle_{AB}$. Both can be measured directly in a path sampling run. For comparison we compute $v(\tau)$ and $\tilde{k}(\tau)$ also from a Brownian dynamics trajectory by averaging over all trajectory segments connecting A and B in $L=199$ time steps. The normalized correlation function $\tilde{k}(\tau)$ for the high friction limit is shown in Fig. 7 (top figure). The agreement is very good, which is expected considering the results discussed in the previous subsection. In Fig. 7 (bottom figure) we plotted $v(\tau)$ for the straightforward and the dynamic path sampling algorithm. As taking the derivative of $\tilde{k}(\tau)$ increases the error the agreement is slightly worse. Clearly, $\nu(\tau)$ reaches a plateau after $\tau=150$, which is required for a good estimate of the rate constant. The average value at the plateau is $\nu(\tau)\approx 0.076$.

The sudden increase of $\langle \dot{h}_B(\tau)\rangle$ towards the end of the

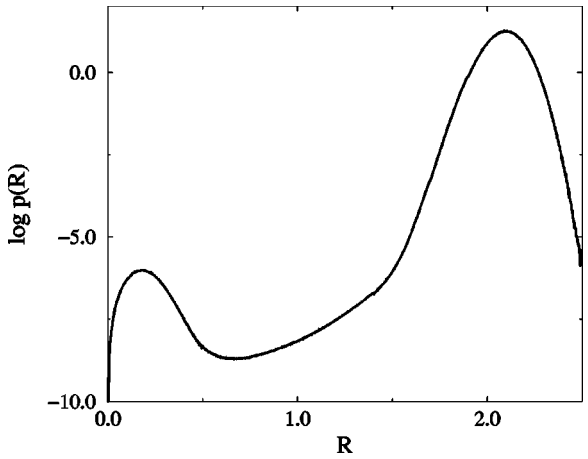

FIG. 8. Logarithm of the probability to find the endpoint x_L of the path of length $L=199$ at a distance R from the center of the final region. $p(R)$ is normalized such that $\int_0^\infty p(R)dR=1$.

path requires comment. In deriving Eq. (26) we have assumed that once the system has reached region B is stays there for a long time compared to the molecular time scale t_{mol}. This is to say that $\langle h_A(x_0)h_B(x_\tau)h_{\tilde{B}}(x_L)\rangle=0$, where $h_{\tilde{B}}(x)=0$ if x is in B and $h_{\tilde{B}}(x)=1$ if x is outside B. This is, however, not exactly true, because a small fraction of all trajectories reaching B at a time slice $\tau<L$ escape again from B before $\tau=L$. These trajectories contribute to $\langle h_A(x_0)h_B(x_\tau)\rangle$ but are not seen by the path sampling method, which by construction generates only trajectories ending in B. This effect is larger at the end of the path and is further amplified by the differentiation with respect to τ. Since, as shown by our numerical results, the sudden increase of $\langle \dot{h}_B(\tau)\rangle$ occurs only at the end of the path after the plateau is reached, it does not affect the estimation of rate constants. Furthermore, the relative size of this sudden increase will decrease as the overall rate constant for the process decreases.

Part two in the calculation of the rate constant is the estimation of the probability $P(L)$ in Eq. (25), or equivalently the isomorphic reversible work $W(L)$ needed to drag the path over the barrier to the final region. Defining the parameter λ as the distance R of the endpoint x_L of the path to the center of the final region, we performed path simulations for six different windows: $0\leqslant R\leqslant 0.5$, $0.5\leqslant R\leqslant 1.0$, $1.0\leqslant R\leqslant 1.4$, $1.4\leqslant R\leqslant 1.7$, $1.7\leqslant R\leqslant 1.9$, and $1.9\leqslant R\leqslant 2.5$. These values were chosen such that the whole window was sampled with accurate statistics. The value of R was monitored and histogrammed during the path simulation. In Fig. 8 we show the logarithm of the probability $p(R)$ to find the endpoint at a certain R. The histograms for the different windows were matched together by multiplying with a constant. $p(R)$ is normalized such that $\int_0^\infty p(R)dR=1$. Integration of the normalized $p(R)$ over the final region B gives a factor of $P(L)=0.00068$. Multiplying this with $\nu(L)=0.076$ gives the desired rate constant $k_{A\to B}=5.13\times 10^{-5}$. We can compare this result with a straightforward measurement of $k(L)$ which gives $k_{A\to B}=5.12\times 10^{-5}$.

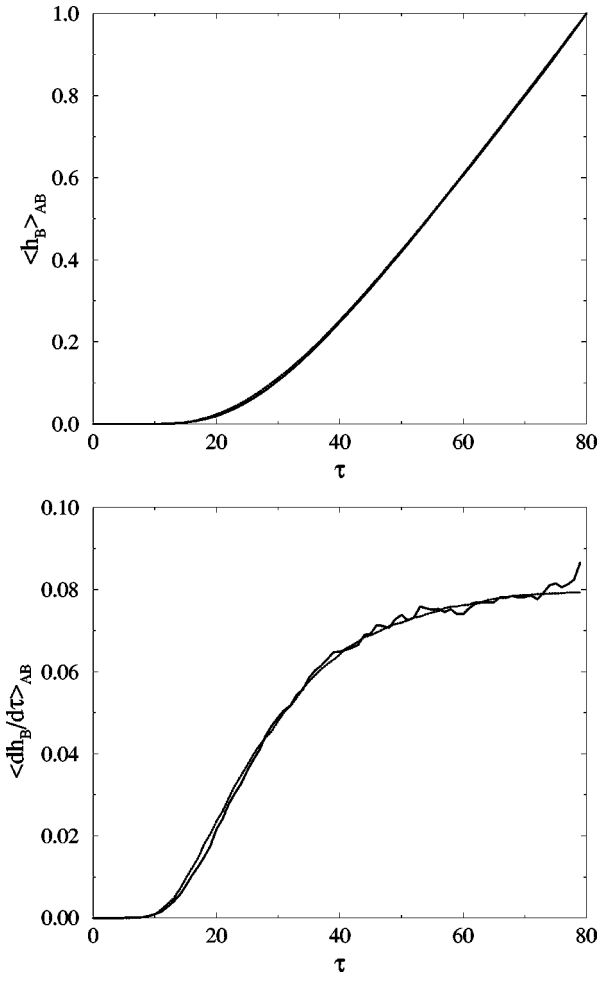

FIG. 9. Normalized correlation function $\langle h_B(x_\tau)\rangle_{AB}$ (top figure) and its time derivative $\langle \dot{h}_B(x_\tau)\rangle_{AB}$ (bottom figure) along transition paths of length $L=80$ for Langevin dynamics including inertial terms. The index τ numbers the time slices. The solid line refers to results of a path sampling simulation whereas the dotted line was obtained from a Brownian dynamics trajectory. For both simulations $\beta=8$ and $\gamma=2.5$.

Case 2: In Fig. 9, we display the correlation functions $\tilde{k}(\tau)$ and $\nu(\tau)$, respectively, for both straightforward and path simulation of the full Langevin equation. Both methods are again in full agreement with each other. The plateau in $\nu(\tau)$ is reached after 80 time steps and has a value of $\nu(\tau)\approx 0.08$.

In this case we use the thermodynamic integration method as introduced in Sec. IV to calculate the factor $P(L)$ of the rate constant. The derivative dW/dR is plotted in Fig. 10 as a function of R. Integration of this curve from $R=0.7$ to $R\to\infty$ yields $\Delta W=7.75\pm 0.37$ corresponding to $P(L)=0.00043(0.00030-0.00062)$, where the values in the brackets are the lower and upper bounds of $P(L)$. Multiplying this with $\nu(L)$ gives an estimate rate constant $k_{A\to B}=3.4\times 10^{-5}(2.4\times 10^{-5}-5.0\times 10^{-5})$. We can compare this result with a straightforward measurement of $k(L)$ which gives $k_{A\to B}=4.1\times 10^{-5}$.

For comparison, we also measured the probability $p(R)$ to find the endpoint of the path at a distance R from the center of the final region. Integration leads to $P(L)$

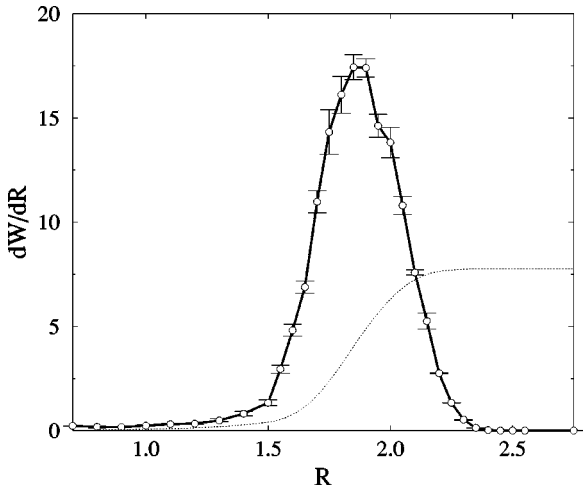

FIG. 10. Derivative dW/dR of the reversible work W with respect to the radius R of the final region B as a function of R. Integrating over dW/dR (dotted line) one obtains the reversible work necessary to shrink the final region from infinity to a radius of $R=0.7$. The magnitude of the error bars was estimated from the mean square deviation of the results obtained from 16 independent simulations of 10^6 integration steps. For $\beta=8$ and $\gamma=2.5$ and a path length of $L=80$ the thermodynamic integration yields $\langle h_A(x_0)h_B(x_L)\rangle=0.00043(0.00030-0.00062)$ This value agrees well with $\langle h_A(x_0)h_B(x_L)\rangle=0.00052$ as obtained from a Brownian dynamics trajectories of 10^9 steps with step size $\Delta t=0.25$.

$=0.00049$ which corresponds to a rate constant of $k_{A\to B}=3.9\times10^{-5}$. This value is in good agreement with the rate constant obtained from the Brownian dynamics trajectory. We note that to obtain a given accuracy the thermodynamic integration method requires a larger number of individual simulations than the umbrella sampling method. The latter is therefore the more efficient of the two for the calculation of the probability $P(L)$.

VI. CONCLUSIONS

In this paper, we have introduced methods to generate and sample an ensemble of transition paths. The paths evolve according to a stochastic dynamics (Metropolis Monte Carlo or Brownian dynamics) and conserve the Boltzmann distribution. The stochasticity allows the definition of an action for transition paths, which can be sampled by molecular dynamics or by Monte Carlo methods. We apply these ideas to a simple barrier crossing problem, where we show that the transition path ensemble reproduces the results of standard simulations by determining energy profiles, energy fluctuations, and rate constants for transition paths.

The Metropolis transition probability allows a relatively large step size and is applicable to discrete systems, like the Ising model. However, the repeated calculation of the rejection factor $Q(r)$ makes the Metropolis transition probability computationally expensive for systems which do not allow an efficient estimation of $Q(r)$. Both the Metropolis and the high friction Langevin dynamics assume that the momenta equilibrate at each time slice, and that the configurational part of phase space effectively dictates the time evolution. In contrast, in the full Langevin equation the variation of the friction can be used in principle to study the approach to the Newtonian limit.

The local algorithm is conceptually simple and easy to implement. As a consequence of the single particle moves, one finds that the algorithm scales as L^3. The CBMC algorithm is applicable to high-dimensional systems, in particular to solvation problems, where only a subset of the system is constrained. The performance depends strongly on an intelligent choice for the guiding field. In situations with a high energy barrier and with a poorly chosen guiding field, CBMC fails for the same reason as straightforward sampling, i.e., the acceptance rate becomes very low. Dynamical sampling schemes are motivated by the need to make collective moves to improve on the L^3 scaling. For the dynamical algorithm, one finds the scaling law L^2. Unfortunately, the singular part in the Metropolis transition probability leads to difficulties in deriving a dynamical algorithm for Metropolis paths.

If the dynamical algorithm is used to sample Langevin paths for a low friction coefficient and/or at a low temperature, severe computational problems may occur. In these cases the path forces become very strong and the associated high frequency modes require a small integration time step, slowing down the simulation. In addition, a high randomization rate of the momenta is necessary to achieve ergodicity in spite of the near integrability of the path Hamiltonian in the low friction limit. As a consequence, the path moves through path space very slowly, leading to long correlation times and a slow convergence of the averages. Multiple time step methods[36] and hybrid MC algorithms[37] are possible methods for avoiding these problems when they may appear at low friction and low temperature.

Rate constants are calculated by measuring the reactive flux in the transition path ensemble and combining it with the reversible work required to stretch a path to the final endpoint region. Exploiting the similarity to conventional free energy methods, we performed umbrella-sampling and thermodynamic integration to determine the rate constant in our model problem. We note that in more complex problems the order at which the umbrella sampling for the different regions is carried out might have an influence on the results. Specifically, there might be a difference in the reversible work depending on whether a free path is gradually confined to the final region or the final constraint on the path is gradually released. The size of the resulting hysteresis can be useful in estimating the accuracy of the reversible work calculation.

Summarizing, the transition path method finds reaction paths by sampling the path ensemble, rather than requiring the *a priori* specification of a reaction coordinate, and it handles situations with several transition states. In addition, one can estimate the rate constant of the dynamical process. It is, however, computationally expensive and should not be applied if alternative methods are available.

In future papers, we will report on the application of this approach to high-dimensional systems.

ACKNOWLEDGMENTS

This work was initiated with support from the National Science Foundation and completed with support from the Department of Energy through the Chemical Sciences Division of Lawrence Berkeley National Laboratory. The calculations reported in this work were partly done on the Cray T3E at Lawrence Berkeley National Laboratory. C. Dellago gratefully acknowledges support from the Austrian Fonds zur Förderung der wissenschaftlichen Forschung Grant No. J01302-PHY.

APPENDIX A: INTEGRATING THE LANGEVIN EQUATION

In a practical simulation, the Langevin equations of motion are integrated numerically by assuming that the systematic part of the force is constant or varies linearly during a short time step. For systematic forces varying linearly, one obtains a Verlet-like algorithm:[20]

$$r(t+\Delta t)=r(t)+c_1\Delta t v(t)+c_2\Delta t^2 a(t)+\delta r_R, \tag{A1}$$

$$v(t+\Delta t)=c_0 v(t)+(c_1-c_2)\Delta t a(t)+c_2\Delta t a(t+\Delta t)+\delta v_R,$$

where δr_R and δv_R are the random displacements in configuration and velocity space distributed according to (9). Δt is the integration time step and the acceleration $a(t)=F[r(t)]/m$. We note that in the limit of vanishing friction this scheme reduces to the velocity Verlet algorithm. The coefficients appearing in the integration formula are

$$c_0=e^{-\gamma\Delta t},$$

$$c_1=(1-e^{-\gamma\Delta t})/\gamma\Delta t=(1-c_0)/\gamma\Delta t, \tag{A2}$$

$$c_2=[1-(1-e^{-\gamma\Delta t})/\gamma\Delta t]/\gamma\Delta t=(1-c_1)/\gamma\Delta t.$$

In the high friction the assumption of constant forces F during the time step Δt leads to the finite difference equation

$$r(t+\Delta t)=r(t)+\frac{\Delta t}{m\gamma}F(r)+\delta r_R, \tag{A3}$$

where the random displacement δr_R is distributed according to (12).

APPENDIX B: MONTE CARLO ALGORITHMS

1. Local algorithm

In analogy to the derivation in the text, we derive the acceptance rules for the endpoints of the path. For the initial time slice we use the generating probability

$$P_{\rm gen}[r_0']=\frac{g(r_0,r_0')+\delta(r_0'-r_1)Q(r_1)}{|g|(r_0)+Q(r_1)}h_A(r_0'), \tag{B1}$$

which leads to the acceptance probability

$$P_{\rm acc}[r_0\to r_0']=\min[1,A/B];$$

$$A=\begin{cases} e^{-\beta E(r_0')}\omega(r_0\to r_1), & \text{if } r_0'\neq r_1; \\ e^{-\beta E(r_0')}g(r_0,r_0'), & \text{if } r_0'=r_1. \end{cases}$$

$$B=\begin{cases} e^{-\beta E(r_0)}\omega(r_0\to r_1), & \text{if } r_0\neq r_1; \\ e^{-\beta E(r_0)}g(r_0,r_0'), & \text{if } r_0=r_1. \end{cases} \tag{B2}$$

The same construction for the last time slice gives

$$P_{\rm gen}[r_L']=\frac{g(r_L,r_L')+\delta(r_L'-r_{L-1})Q(r_{L-1})}{|g|(r_L)+Q(r_{L-1})}h_A(r_L'), \tag{B3}$$

with the acceptance probability

$$P_{\rm acc}[r_L\to r_L']=\min[1,A/B];$$

$$A=\begin{cases} \omega(r_{L-1}\to r_L'), & \text{if } r_L'\neq r_{L-1}; \\ g(r_L,r_L'), & \text{if } r_L'=r_{L-1}. \end{cases}$$

$$B=\begin{cases} \omega(r_{L-1}\to r_L), & \text{if } r_L\neq r_{L-1}; \\ g(r_L,r_L'), & \text{if } r_L=r_{L-1}. \end{cases} \tag{B4}$$

2. Configurational bias Monte Carlo

For paths with a final endpoint constraint we follow an idea by Garel and Orland.[22,23] We augment the product of transition probability by a factor which biases the evolution of the path towards region B:

$$\prod_{\tau=0}^{L-1} p(r_\tau\to r_{\tau+1})=\prod_{\tau=0}^{L-1}[p(r_\tau\to r_{\tau+1})B(r_\tau,r_{\tau+1})], \tag{B5}$$

where $B(r_\tau,r_{\tau+1})=e^{\phi_\tau(r_\tau)-\phi_{\tau+1}(r_{\tau+1})}$ depends on the guiding field ϕ_τ, which can be any function satisfying $\phi_0=0$ and $\phi_L=0$. The generating probability becomes

$$\tilde{P}_{\rm gen}[r_\tau^{(i)}]=\frac{\min[1,e^{-\beta(E(r_\tau^{(i)})-E(r_{\tau-1}))}]B[r_{\tau-1},r_\tau^{(i)}]+\delta(r_{\tau-1}-r_\tau^{(i)})Q^{\rm est}(r_{\tau-1})B[r_{\tau-1},r_{\tau-1}]}{\tilde{w}[r_\tau]}, \tag{B6}$$

where

$$\tilde{w}[r_\tau]=\frac{1}{k}\sum_{j=1}^{k}\min[1,e^{-\beta(E(r_\tau^{(j)})-E(r_{\tau-1}))}]B[r_{\tau-1},r_\tau^{(j)}]$$
$$+Q^{\mathrm{est}}(r_{\tau-1})B[r_{\tau-1},r_{\tau-1}]. \tag{B7}$$

For finite k the estimated rejection factor $Q^{\mathrm{est}}(r)$ is

$$Q^{\mathrm{est}}(r)=1-\frac{1}{k}\sum_{i=1}^{k}\min[1,e^{-\beta(E(r^{(i)})-E(r))}]; \tag{B8}$$

the trial moves $r^{(i)}$ are taken from the probability distribution $\eta(r,r^{(i)})$. The Rosenbluth weight $\tilde{W}_a$ for this algorithm can be obtained by considering the ratio e^{-S_a}/P_a, where $P_a=\Pi_{\tau=0}^{L-1}\tilde{P}_{\mathrm{gen}}(r_\tau^a)$ is the total generating probability for a path a, and e^{-S_a} is its path action:

$$\tilde{W}_a=e^{-S_a}/P_a=e^{-\beta E(r_0)}\prod_{\tau=0}^{L-1}\frac{\tilde{w}[r_\tau^a]}{B(r_\tau^a,r_{\tau+1}^a)}$$
$$=e^{-\beta E(r_0)}\prod_{\tau=0}^{L-1}\tilde{w}[r_\tau^a] \tag{B9}$$

(using the boundary constraints for ϕ_0 and ϕ_L in the last line). The acceptance probability becomes $P_{\mathrm{acc}}[a\to b]=\min[1,\tilde{W}_b/\tilde{W}_a]$. Obviously, all paths begin in region A and are only accepted if they reach region B.

The choice for the guiding field strongly affects the efficiency of the simulation. We have tested two ideas: a guiding field which ''pulls'' the directed path towards the final region, and a guiding field which rescales the Boltzmann factor to facilitate successful transitions. In the first case, a simple choice is

$$\exp\{-\phi_\tau(r_\tau)\}=\begin{cases}1, & \text{if } \tau=0 \text{ or } \tau=L;\\ \exp\{-(r_\tau-r^*)^2/2\sigma^2(L-\tau)\} & \text{otherwise.}\end{cases} \tag{B10}$$

In this case, r^* is a point in the final region. For the second case, we define a constant β^* such that $0<\beta^*<\beta$ and sample paths for an effective inverse temperature $\beta-\beta^*$:

$$\exp\{-\phi_\tau(r_\tau)\}=\begin{cases}1, & \text{if } \tau=0 \text{ or } \tau=L;\\ \exp\{+\beta^* V(r_\tau)\} & \text{otherwise.}\end{cases} \tag{B11}$$

This choice does not make any assumptions on the actual form of the reaction coordinate. It is also possible to combine the two approaches by using a linear combination of the above ϕ_τ's.

In contrast to standard (polymer) configurational bias sampling, we do not apply the condition of ''super-detailed balance'' for directed paths. Super-detailed balance states that for any set of trial moves around the old and new conformation, detailed balance has to be satisfied.[35] In the case of transition path sampling, one constructs the rejection factor $Q^{\mathrm{est}}(r)$ on the fly. Therefore, a large enough upper summation limit k is needed to estimate the rejection probability $Q(r)$. This point may be verified either by studying the convergence of $Q(r)$ with increasing k, or by comparing directed paths with standard MC runs (see Sec. V).

APPENDIX C: DYNAMICAL ALGORITHMS

In this appendix we calculate the path forces $-\nabla_X S$ necessary to integrate the equations of motion (21). Since for the singular transition probability (4a) the derivatives of the action cannot be evaluated, in the following paragraphs we restrict ourselves to the Langevin transition probability (8). We also explain how to treat the endpoints of the path confined to the corresponding boundary regions.

Different forces arise from the different terms in the action (23). The canonical distribution of the first time slice is the origin of the following path force acting on the first copy of the system:

$$F_0^r=-\beta\partial V(r_0)/\partial r_0,$$
$$F_0^v=-\beta m v_0, \tag{C1}$$

where the superscripts r and v denote the spatial and velocity components of the generalized force, respectively. Next, we calculate the path forces arising from the links $\log p(x_\tau\to x_{\tau+1})$ for the Langevin probabilities (9). By differentiation we obtain

$$\frac{\partial\log p}{\partial r_\tau^\alpha}=\frac{1}{(1-c_{rv}^2)}\left\{\frac{1}{\sigma_r^2}\left(\delta r_R^\alpha+c_2\frac{\Delta t^2}{m}\sum_\beta\delta r_R^\beta D_\tau^{\beta\alpha}\right)\right.$$
$$+\frac{1}{\sigma_v^2}(c_1-c_2)\frac{\Delta t}{m}\sum_\beta\delta v_R^\beta D_\tau^{\beta\alpha}$$
$$-\frac{c_{rv}}{\sigma_r\sigma_v}\left[\delta v_R^\alpha+c_2\frac{\Delta t^2}{m}\sum_\beta\delta v_R^\beta D_\tau^{\beta\alpha}\right.$$
$$\left.\left.+(c_1-c_2)\frac{\Delta t}{m}\sum_\beta\delta r_R^\beta D_\tau^{\beta\alpha}\right]\right\}, \tag{C2}$$

and

$$\frac{\partial\log p}{\partial v_\tau^\alpha}=\frac{1}{(1-c_{rv}^2)}\left\{\frac{c_1\Delta t\,\delta r_R^\alpha}{\sigma_r^2}+\frac{c_0\delta v_R^\alpha}{\sigma_v^2}\right.$$
$$\left.-\frac{c_{rv}}{\sigma_r\sigma_v}(c_1\Delta t\,\delta v_R^\alpha+c_0\delta r_R^\alpha)\right\}, \tag{C3}$$

where

$$D_\tau^{\beta\alpha}=-\left.\frac{\partial^2 V}{\partial r^\alpha\partial r^\beta}\right|_{r_\tau} \tag{C4}$$

is the matrix of the second derivatives of the interaction potential of the system. The derivatives of $\log p(x_\tau\to x_{\tau+1})$ with respect to $x_{\tau+1}$ are

$$\frac{\partial\log p}{\partial r_{\tau+1}^\alpha}=-\frac{1}{(1-c_{rv}^2)}\left\{\frac{\delta r_R^\alpha}{\sigma_r^2}-\frac{c_2\Delta t}{m\sigma_v^2}\sum_\beta\delta v_R^\beta D_{\tau+1}^{\beta\alpha}\right.$$
$$\left.-\frac{c_{rv}}{\sigma_r\sigma_v}\left(\delta v_R^\alpha-c_2\frac{\Delta t}{m}\sum_\beta\delta r_R^\beta D_{\tau+1}^{\beta\alpha}\right)\right\}, \tag{C5}$$

and

$$\frac{\partial \log p}{\partial v_{\tau+1}^{\alpha}} = -\frac{1}{(1-c_{rv}^2)}\left\{\frac{\delta v_R^{\alpha}}{\sigma_v^2} - \frac{c_{rv}}{\sigma_r \sigma_v}\delta r_R^{\alpha}\right\}. \tag{C6}$$

In the high friction limit derivatives of the transition probability (12) are given by

$$\frac{\partial \log p}{\partial r_{\tau}^{\alpha}} = \frac{1}{\sigma_r^2}\left(\delta r_R^{\alpha} + \frac{\Delta t}{m\gamma}\sum_{\beta}\ \delta r_R^{\beta} D_{\tau}^{\beta\alpha}\right), \tag{C7}$$

$$\frac{\partial \log p}{\partial r_{\tau+1}^{\alpha}} = \frac{-1}{\sigma_r^2}\delta r_R^{\alpha}. \tag{C8}$$

Also the initial and final constraint exert forces on the path. If we use smooth approximations of the characteristic functions h_A and h_B the constraints generate smooth forces on the path. These forces can be simply added to the forces originating from the transition probabilities and the canonical distribution in the first time slice. However, if the initial and final regions A and B are characterized by the functions (3) the corresponding forces become singular. In this case

$$-\log h_{A,B}(x) = \begin{cases} 0, & \text{if } x \in A,B, \\ \infty & \text{if } x \notin A,B, \end{cases} \tag{C9}$$

and the initial and final constraints correspond to hard containers confining the initial and final time slice to their respective regions. Hence, a different approach to determine the trajectory of the path must be adopted. For hard-wall containers the equations of motion are integrated without boundary constraints. As soon as either the initial or the final copy of the system crosses the boundary of the corresponding region A or B the exact collision point with the region boundary has to be determined. This can be done, for example, with an interval bisection method. At the collision the path coordinates X do not change. The corresponding path momenta are specularly reflected at the container boundary and change according to

$$P \to P - 2(P\cdot\hat{n})\hat{n}, \tag{C10}$$

where $\hat{n}$ is a unit vector normal to the container boundary at the collision point. $\hat{n}$ points into the container. This reflection operation conserves the kinetic path energy. If the boundary of the container is defined by some function $f(x)=0$, the normal vector at the collision point is

$$\hat{n} = -\nabla_x f(x)/|\nabla_x f(x)|. \tag{C11}$$

Thus, the whole path trajectory consists of smooth streaming segments punctuated by impulsive hard collisions of the initial and final system copy with their respective container walls.

[1] P. Hänggi, P. Talkner, and M. Borkovec, Rev. Mod. Phys. **62**, 251 (1990); B. J. Berne, in *Multiple Time Scales*, edited by J. U. Brackbill and B. I. Cohen (Academic Press, New York, 1985), pp. 419–436.

[2] J. C. Keck, Discuss. Faraday Soc. **33**, 173 (1962); J. C. Keck, Adv. Chem. Phys. **13**, 85 (1967); J. B. Anderson, J. Chem. Phys. **58**, 4684 (1973); C. H. Bennett, in *Algorithms for Chemical Computations*, ACS Symposium Series No. 46, edited R. E. Christofferson (American Chemical Society, Washington, D.C., 1977), p. 63.

[3] D. Chandler, *Introduction to Modern Statistical Mechanics* (Oxford University Press, New York, 1987).

[4] D. Chandler, J. Chem. Phys. **68**, 2959 (1978).

[5] J. McIver and A. Komornicki, J. Am. Chem. Soc. **94**, 2625 (1972).

[6] C. J. Cerjan and W. H. Miller, J. Chem. Phys. **75**, 2800 (1981); F. Jensen, *ibid.* **102**, 6706 (1995).

[7] K. Müller, Angew. Chem. Int. Ed. Engl. **19**, 1 (1980).

[8] R. Czerminski and R. Elber, J. Chem. Phys. **92**, 5580 (1990); R. Elber, D. P. Chen, D. Rojewska, and R. Eisenberg, Biophys. J. **68**, 906 (1995).

[9] L. R. Pratt, J. Chem. Phys. **85**, 5045 (1986).

[10] R. Elber and M. Karplus, Chem. Phys. Lett. **139**, 375 (1987).

[11] E. M. Sevick, A. T. Bell, and D. N. Theodorou, J. Chem. Phys. **98**, 3196 (1993).

[12] R. Czerminski and R. Elber, Int. J. Quantum Chem. **24**, 167 (1990).

[13] G. Mills and H. Jónsson, Phys. Rev. Lett. **72**, 1124 (1994).

[14] R. E. Gillilan and K. R. Wilson, J. Chem. Phys. **97**, 1757 (1992).

[15] E. A. Carter, G. Ciccotti, J. T. Hynes, and R. Kapral, Chem. Phys. Lett. **156**, 472 (1989).

[16] D. Chandler, in *Les Houches 51, Part 1, Liquids, Freezing and Glass Transition*, edited by D. Levesque, J. P. Hansen, and J. Zinn-Justin (Elsevier, New York, 1991).

[17] D. M. Ceperley, Rev. Mod. Phys. **67**, 279 (1995).

[18] N. Metropolis, A. W. Rosenbluth, M. N. Rosenbluth, A. H. Teller, and E. Teller, J. Chem. Phys. **21**, 1087 (1953).

[19] S. Chandrasekhar, Rev. Mod. Phys. **15**, 1 (1943).

[20] M. P. Allen and D. J. Tildesley, *Computer Simulation of Liquids* (Clarendon, Oxford, 1987).

[21] M. N. Rosenbluth and A. W. Rosenbluth, J. Chem. Phys. **23**, 356 (1955); J. I. Siepmann and D. Frenkel, Mol. Phys. **75**, 59 (1992); J. J. de Pablo, M. Laso, and U. W. Suter, J. Chem. Phys. **96**, 2395 (1992); D. Frenkel, G. C. A. M. Mooij, and B. Smit, J. Phys. Condensed Matter **4**, 3053 (1992).

[22] T. Garel and H. Orland, J. Phys. A **23**, L621 (1990).

[23] P. G. Higgs and H. Orland, J. Chem. Phys. **95**, 4506 (1991); B. Velikson, T. Garel, J.-C. Niel, H. Orland, and J. C. Smith, J. Comput. Chem. **13**, 1216 (1992).

[24] M. Parrinello and A. Rahman, J. Chem. Phys. **80**, 860 (1984); M. E. Tuckerman, B. J. Berne, G. J. Martyna, and M. L. Klein, *ibid.* **99**, 2796 (1993).

[25] J. Polonyi and H. W. Wyld, Phys. Rev. Lett. **51**, 2257 (1983); S. Sorella, S. Baroni, R. Car, and M. Parrinello, Europhys. Lett. **8**, 663 (1989).

[26] D. Bohm and E. P. Gross, Phys. Rev. **75**, 1864 (1949).

[27] J. A. Montgomery, D. Chandler, and B. J. Berne, J. Chem. Phys. **70**, 4056 (1979).

[28] H. C. Andersen, J. Chem. Phys. **72**, 2384 (1980).

[29] M. J. Gillan, Philos. Mag. A **58**, 257 (1988).

[30] S. Nosé, J. Chem. Phys. **81**, 511 (1984); W. G. Hoover, Phys. Rev. A **31**, 1695 (1985).

[31] W. G. Hoover and B. L. Holian, Phys. Lett. A **211**, 253 (1996).

[32] W. G. Hoover, A. J. C. Ladd, and B. Moran, Phys. Rev. Lett. **48**, 1818 (1982).

[33] D. J. Evans, J. Chem. Phys. **78**, 3297 (1983).

[34] G. M. Torrie and J. P. Valleau, J. Comput. Phys. **23**, 187 (1977).

[35] D. Frenkel and B. Smit, *Understanding Molecular Simulation* (Academic Press, San Diego 1996.

[36] M. Tuckerman, B. J. Berne, and G. J. Martyna, J. Chem. Phys. **97**, 1990 (1992).

[37] S. Duane, A. D. Kennedy, B. J. Pendleton, and D. Roweth, Phys. Lett. B **195**, 216 (1988).